An Investigation into the Feasibility of a Sea Water Based Acoustic UHE Neutrino Telescope

Simon Bevan

Supervised by Dr.David Waters

June 8, 2006

Abstract

Using acoustic techniques, it is hoped that a new type of telescope can be developed to search for UHE ($> 10^{10}$ GeV) neutrinos. Using an 8 hydrophone array, ACoRNE is investigating the practicality of such acoustic telescope. This paper will report on the progress of this investigation, focusing mainly on data analysis and event reconstruction, with the aim of reducing the acoustic background at Rona.

Contents

1 UHE Neutrino Astronomy

1.1 Theory

Most modern techniques rely on the use of the electromagnetic spectrum (radio, infrared, visible, ultraviolet, x-ray, and most recently gamma rays) to study the universe, but new techniques are being developed to study the universe via an alternative particle, the neutrino. This method is still in its infancy, but if the new techniques prove to be successful many of the unanswered questions in astrophysics today could be answered.

1.2 Why the Neutrino

The neutrino is electrically neutral, only interacts through the weak nuclear force, and has an extremely small cross section, and hence interacts with matter very rarely.

The neutrino is the second most abundant particle in the universe, with a number density of $3.10^6/\mathrm{m}^3$ (number one, the photon which has a number density of $1.10^7/\mathrm{m}^3$, and the proton is behind with only $0.5/\mathrm{m}^3$). However this number, the neutrino density, is completely dominated by relic neutrinos from the big bang. These relic neutrinos are very low energy and are directly unobservable (with current techniques). The remainder higher energy neutrinos, for the reasons stated above, are still very difficult to detect, but the potential of neutrino telescopes are now investigated.

Whereas nuclear energy (MeV) neutrino astronomy has been well established[1], the low cross section and poor angular resolution of MeV neutrinos has always been a problem in advancing the techniques to much beyond the Sun and nearby supernovae. Major efforts have been made in advancing this field (AMANDA, ANTARES, ICECUBE), but all major experiments to date have been optimised for lower energies than the new proposed neutrino telescopes, which are aiming to detect ultra-high energy (UHE) neutrinos (Energy $> 10^{10}$ GeV).

Using UHE neutrinos has the advantages that, i) the increase of the neutrino cross-section, and angular resolution with energy, and ii) the opportunity to use large natural target material (water, salt, ice). Detection at energies of this magnitude is difficult with conventional optical neutrino detectors, as they are optimised for detection of Cerenkov radiation, which has an attenuation length of 50-100m, depending on the material. Therefore the arrays are km^3, and with the magic number being 1 UHE neutrino per km^3 per year, the arrays are simply too small to be good detectors of UHE neutrinos. In order to detect these high energies new many km^3 detectors are being designed[2].

There are many methods of detecting UHE neutrinos that are being investigated. This report will focus solely on the detection of UHE neutrinos by the detection of the acoustic pulse generated when the neutrino interacts with water - acoustic detection.

1.3 Other Detection Methods

There are also other types of neutrino detectors, namely optical Cerenkov, air shower detectors, and radio Cerenkov. Radio Cerenkov is hoping for the same energies as acoustic detection, but the optical Cerenkov is optimised for lower energies. Air shower detectors hope detect at as high energies as acoustic but are not optimised for neutrino detection. It is hard for air shower detectors to distinguish the type of shower that occurred. Fig 1 shows the energy range for these other types of detectors.

1.4 What are the Aims of Neutrino Astronomy?

High-energy astronomy has been much advanced with the invention of the gamma ray telescope[3], but the range of modern high-energy gamma ray telescopes is limited. This is because of attenuation of gamma rays from distant sources. At a few hundred TeV, gamma rays do not survive the journey from the centre of our galaxy. At 10^{14}eV they interact with the cosmic background

radiation, and annihilate into an electron pair, equation 1. Neutrino astronomy aims to look into cosmological interesting distances, as neutrinos suffer no such interactions.

$$\gamma + \gamma_{BK} \rightarrow e^+ + e^- \tag{1}$$

With UHE neutrino astronomy we could look into the densest places of the universe hidden to current techniques. UHE neutrino astronomy could also help prove or dismiss many of the current problems in astro-particle physics today. For example it would be able to see the to-date unseen details of the ultimate energy release during the collapse of matter, the origin of cosmic rays, and could even give crucial insights into the nature of dark matter.

Another important advantage of using neutrinos, is the ability to distinguish between electromagnetic and hadronic processes. Accelerated electrons and protons both result in the production of high energy cosmic rays, but only hadronic processes result in the production of neutrinos.

1.5 Potential Sources of UHE Neutrinos

The origin and mechanism for accelerating UHE cosmic rays remains one of the major unknown phenomena in astrophysics. Isolated sources of UHE neutrinos are believed to be produced by protons accelerated in highly energetic environments colliding with the ambient gas and radiation surrounding the accelerating environments. The neutrinos are produced through proton-proton or proton-photon interactions via pion production and decay. Such accelerators [4] might be an active galactic nuclei, AGN, powered by a super massive black hole, gamma ray bursts, or in shock fronts of supernovae remnants, micro-quasars, and magnetars.

1.6 Predictions of Expected Flux

Predictions have been made for the expected flux of UHE neutrinos based on the standard model of particle physics; namely Waxman-Bachall[5] limit and the GZK cut off.

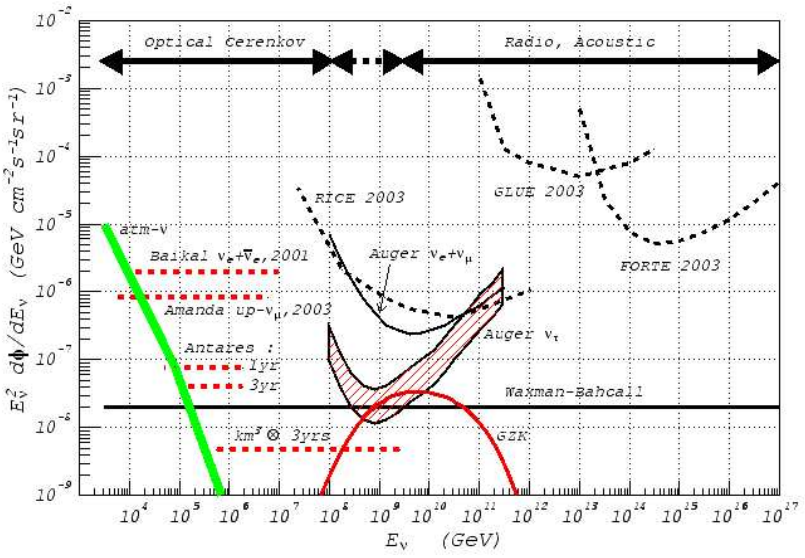

Figure 1: Showing the GZK, Waxman-Bachall, and the atmospheric neutrino flux. The fig also shows the upper limits of other neutrino detectors. The dates refer to the dates of published limits.

Waxman-Bachall limit is 2.10^{-8} E^2(GeV cm^2 sec sr)$^{-1}$ - Derived from photo-meson interactions. The value quoted here is the upper limit.

Mannheim et al[6] corrected the Waxmann Bachall limit and extended the analysis to include cases where the emitted protons suffer adiabatic losses on the large scale, and magnetic fields and absorption processes within the sources. This results in more general bounds allowing much higher extra galactic neutrino fluxes - 1.10^{-6} E^2(GeV cm^2 sec sr)$^{-1}$.

GZK cut-off is the limit of the maximum energy of protons of cosmological origin because of the finite (50Mpc) inelastic collision length of such particles in the cosmic background radiation. The highest energy cosmic rays are energetic enough to have photo-production reactions with the cosmic background radiation. The secondary mesons produced in the photo-production decay into gamma rays and neutrinos. Using a full model of neutrino production due to proton interactions on CMB photons over the full lifetime of the universe, calculations of the flux of GZK neutrinos can be made, fig 1.

$$p + \gamma_{cmb} \rightarrow \pi^+ + n \tag{2a}$$
$$\pi^+ \rightarrow \mu + \nu_\mu \tag{2b}$$
$$\mu \rightarrow e^- + \nu_\mu + \nu_e \tag{2c}$$
$$n \rightarrow p + e^- + \bar{\nu}_e \tag{2d}$$

GZK neutrinos are of significant interest for the early studies of UHE neutrinos, as the measurement of the detected flux can be directly compared with theory. For energies above the GZK cut-off point, comparing the measured flux with theory becomes more difficult, due to lack of theory. But it must be noted that at present this is the only theory there is! It must also be noted that the GZK flux is based on the observed flux ultra high energy proton cosmic rays, and has uncertainties of a factor of 2.

Although fig 1 shows an upper limit for the Waxman-Bahcall flux extending to 1.10^{17}GeV, this is only generated on general arguments about Fermi acceleration in astrophysical objects. This also must have a cut-off at some point, possibly around 10^{21} or 10^{22} eV, but the actual value is unknown.

Other possible models for the neutrino flux at energies above the GZK limit are models in which neutrinos are generated by the decay of extremely massive particles (M $>$ 1.0E14 GeV). These massive particles are thought to be remnants from the very early universe, and have never been detected. Hence any flux calculated from their decay is highly theoretical and based on no actual measurements.

Models based on the decay of massive particles are called "top-down" models. "Bottom-up" models try to explain the extremely high-energy cosmic ray data through more conventional acceleration mechanisms in astrophysical objects.

GZK neutrinos also act as good particles to use in neutrino telescopes. This is because the neutrinos travel in a straight line from their point of origin, and the protons from which they were created are of sufficiently high energy as to also travel in a straight line from their point of origin. For these reasons this investigation is going to focus on the detecting GZK neutrinos, 10^{17}eV $<$ E $<$ 10^{21}eV.

Observations of fluxes above these limits would indicate either independent sources or physics beyond the standard model.

2 Detecting UHE Neutrinos

At UHE neutrino energies the cross section of the neutrino is sufficiently high as for the Earth to become opaque to the neutrinos. Hence the detection is of downward going neutrinos. Opposed to upward going neutrinos as searched for by the lower energy neutrino telescopes. But the lower energy telescopes suffer from a background of neutrinos from the interaction of high energy cosmic rays with the atmosphere, which will not effect UHE neutrino telescopes. The

UHE neutrinos interact with the water, and via deep inelastic scattering a hadronic shower is produced.

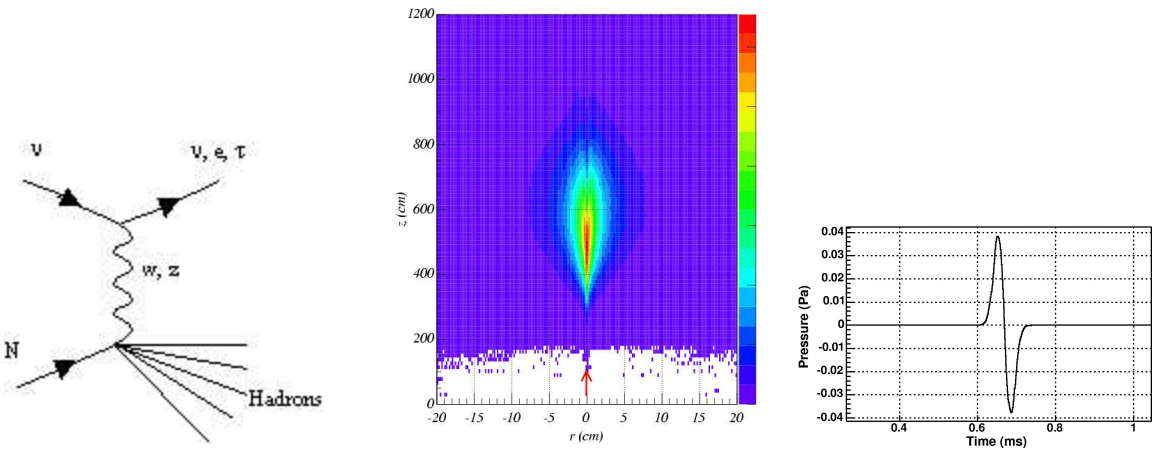

(a) deep inelastic scattering

(b) the energy density of the shower

(c) the acoustic pulse

Figure 2: From interaction to pulse

Hadronic and electromagnetic cascades, produced by the interactions of UHE neutrinos, can deposit sufficient thermal energy, via ionisation losses, in the surrounding medium, fig 2. The heat dissipates only slowly, so the bulk effect is an expansion of the region where the energy was deposited. This in turn produces a bi-polar acoustic pulse with leading compression. The speed of sound in water is much less than the speed of the shower propagation, and the energy deposition along the length of the shower can be considered instantaneous, and hence the radiation adds coherently. This produces a pancake shape acoustic pulse, fig 3.

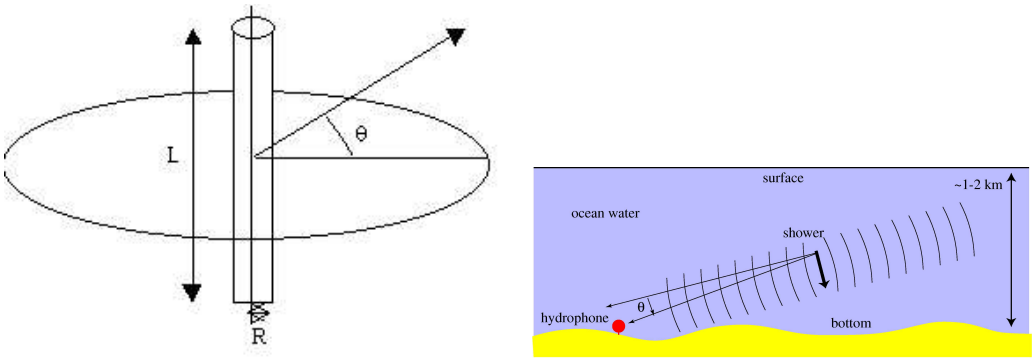

(a) The pancake shaped acoustic pulse

(b) A schematic of the acoustic pulse propagation through the water

Figure 3: acoustic arrays

2.1 Arrays of Detectors

The height of the pressure pulse falls rapidly out of the plane perpendicular to the shower axis, and most of the acoustic energy from a shower is concentrated in a small angular range of roughly ($\theta < |6|^\circ$). Hence a single detector will detect only a small angular range. To overcome this problem an array of detectors has to be used.

At large distances from the shower axis, and in the plane of propagation, the acoustic emission is coherent, giving rise to large amplitude pressure pulses. This gives rise to the main motivation for building acoustic detectors in water - the attenuation length is of the order of kilometres, (10km for components of 10 kHz to about 1km for components of 30 kHz), enabling huge detector volumes to be considered.

Having an array over large volumes of water will improve the counting rate potential by orders of magnitudes compared to that of a single hydrophone. Using an array also has the advantage that the data can be extrapolated to reconstruct the cascade position and the neutrino direction, and can hence be used as a pointer to look for the origin of the UHE neutrinos.

2.2 The Rona Array

Off the island of Rona (west coast of Scotland), the ministry of defence has kindly allowed ACoRNE the use of an eight hydrophone array. From this a continuous stream of data will be taken and the data reduction and reconstruction techniques investigated. The co-ordinates of this array are as follows :

	X	Y	z	Buoy Depth	Extension	Cable length to Shore
CH1	-105	649	225	223	130	3469
CH2	99	654	229	227	128	4300
CH3	-8	397	228	226	30	3855
CH4	-8	3	227	225	130	4033
CH5	-1	-400	219	217	130	4388
CH6	-107	-646	217	215	130	4557
CH7	105	-648	222	220	130	5206
CH8	93	858	224	222	0	3753

Table 1: the positions of the Rona hydrophones

Each hydrophone is attached to a string, which is in turn attached to a mounting plate on the sea bed. These strings are supported by buoys, as illustrated in fig 5. All of the points are relative to some arbitrary point on the surface, which is close to the acoustic centre of the array. The buoy depth is the depth of the buoy that sits above the mounting plate (always 2m above the mounting plate). The extension is the length of the cable between the buoy and the hydrophone. The cable length to shore gives the length of the cable that is run from the mounting plate to the shore station termination unit.

Therefore, for example hydrophone 5, the hydrophone is 130 + 2 meters above the sea bed, with a total cable length to shore of 130 + 2 + 4388 meters.

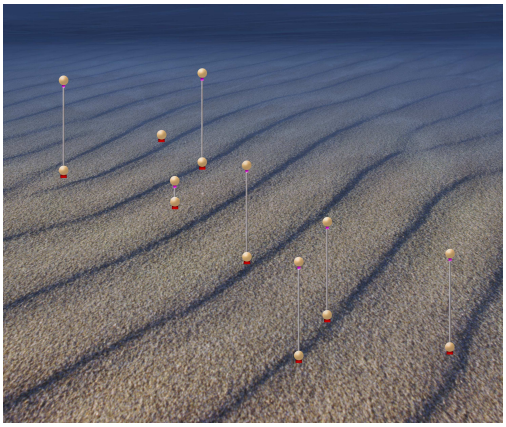

Figure 4: A schematic of the Rona Array

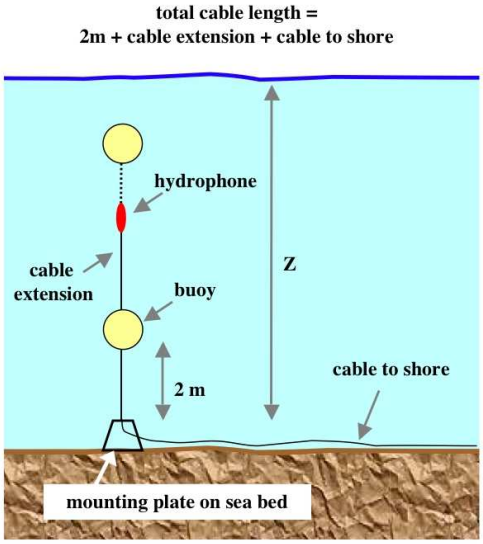

Figure 5: the hydrophone setup

3 Reconstructing Neutrino Events Using a Difference of Time At Arrival Approach

To be able to successfully point back to the neutrino source, the detected event must be reconstructed as accurately as possible. A reconstruction algorithm was developed using a difference of time at arrival approach, see appendix A.

3.1 Testing the Algorithm

To test the reconstruction algorithm, a simple Monte Carlo was created. The Monte Carlo generated 1000 random events in a 1000m radius sphere, with the hydrophone array situated in the centre of this sphere. For every generated event it was assumed that every hydrophone was hit. The times of the hit on each hydrophone was recorded, and fed into the reconstruction code. The results are shown in figure 6.

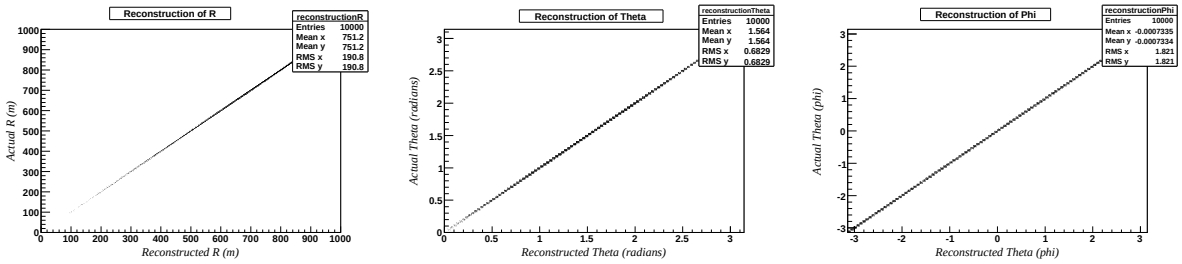

(a) R (b) θ (c) ϕ

Figure 6: Testing the reconstruction algorithm

4 Reducing the Rona Data

ACoRNE has now successfully taken 16 days of continuous data. The format that it is recorded in is simply the continuous output of the 8 hydrophones. This obviously has to reduced into a meaningful form that can be analysed.

- Check the .wav files in the specified directory and loop through each file in turn (should be 8, one for each hydrophone) calculating the length of each file
- The data is then read in in 10s chunks (1.4e6 samples) and filtered with a distortion free high pass filter with a cut off of 2.5kHz
- As each 10s window is read separately, care must be taken to avoid missing coincidences that may happen between two consecutive 10s windows. For the first window, the data is copied into a buffer 1.4e6 + 2000 long, starting at point 2001. The first 2000 points are set to zero. The data is then read from points 2001 until the end. For the second window, it is again copied into a buffer 1.4e6 + 2000 long, starting at point 2001, but this time the contents of the last 2000 points from window one are copied to the first 2000 points in the new buffer, and the coincidence analysis performed. From then on the active trigger window has 1000 leading points and 1000 trailing points. See fig 7
- At the beginning of the buffer a window is created of length 25 samples. The energy is calculated in the window. The window is shifted 25 sample lengths along the buffer and again the energy calculated. This is repeated until the end of the buffer.

- The top 5 most energetic triggers are picked out. This is tagged event type 1 (note that 5 triggers are forced to be considered even though many will not actually be a coincidental acoustic event)
- Differentiate the data (reduces uncorrelated signals)
- Again look at the energy in two adjacent 25 sample blocks
- Pick out the top 5 most energetic events. Tag this as event type 2
- Differentiate again
- Pick out the top 5 most energetic events. Tag this as event type 3
- Now run through a matched filter. A matched filter matches both amplitude and phase to give a theoretically optimal signal to noise ratio. The matched filter that is used here is based on the earlier theoretical calculations that ACoRNE performed on the shape of the pulse expected from the interaction of a UHE neutrino with seawater. It is these calculations that allow a window as small as 25 samples to be used for the calculation of a trigger, as we know that we are looking for a well defined signal.
- Pick out the top 5 most energetic events. Tag this as event type 4
- As there may be replication of events, remove duplicate events (within 500 bins) giving priority to type 4 events, then type 3, then type 2, and lastly type 1
- Save the triggers (1st derivative, as this can most easily integrated and differentiated), with 1000 samples before and after the trigger

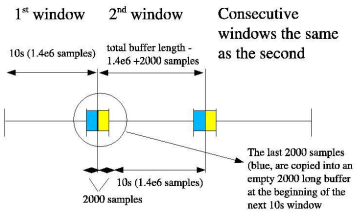

Figure 7: reading in consecutive data files

4.1 Finding Coincident Events

The above reduction in data just gives an array of events for each hydrophone for each ten minute period. But to reconstruct the vertex of an event, the event needs to be recorded on four or more hydrophones in a small time window. This was achieved by:

- Each file (10 minute period) is split into 600 bins (i.e a 1 second bin width). One Second was chosen as it's the transient time of a signal across the array.
- Looping through the triggers sequentially, for each trigger that is fired, the event is placed in the corresponding bin to the time that it occurred, the bin 0.5 seconds above and the bin 0.5 seconds below, eg a trigger at 1.55 seconds will go in bin 2 (1.55s), 3 (2.05s), and bin 2 again (1.05s). This enables every possible combination to be considered, see fig 2.
- This will always put the event into two bins, and one of those bins will contain the event twice. Remove any triggers which are the same from any given bin.
- But for every bin, it could be imagined that the same hydrophone has been triggered more than once. This leaves a combinatorial problem. Therefore every possible combination of events should be considered. This can also prove a great problem. If each hydrophone is

hit only 8 times, this gives a possibility of nearly 17 million different combinations in one bin. This problem is greatly reduced by only considering combinations which fire the same trigger. This assumes that an event always fires the same trigger over the whole array. Therefore for each bin, all combinations of events which fire the same trigger and hit four or more hydrophones are recorded. This is done for trigger type 4, 3, 2, 1, and also mixed triggers. Where for mixed triggers, only the top 1000 most energetic combinations are considered for each bin.

- These events are then reconstructed, using the reconstruction code as described in section 3. Cuts are then made on the causality, is it physically possible for this event to hit the hydrophones that it hit at the time it hit them, the χ^2 (see appendix B), and the direction of the wave, again, is it possible to hit the hydrophones that it did from the direction that it was travelling in . If one combination fails the cuts, the next is considered i.e. if a coincidence of 8 fails, all combinations for a coincidence of 7 (8 in total) from this group are tried. The number of subsets for an 8 fold event would be:
  - 1x8
  - 8x7
  - 28x6
  - 56x5
  - 70x4

	4s	5s	6s
CH1	5.1	5.1, 5.6	5.6
CH2	4.1		5.8
CH3	4.9	4.9, 5.9	5.9
CH4	5.3	5.3	
CH5	3.9		
CH6		5.7	5.7
CH7	5.2	5.2	
CH8		5.8	5.8

(a) Showing hits as they are placed in bins 4, 5, and 6, where the ± has been added and duplicates removed.

5s	5s	5s	5s
5.1	5.6	5.1	5.6
4.9	4.9	5.9	5.9
5.3	5.3	5.3	5.3
5.7	5.7	5.7	5.7
5.2	5.2	5.2	5.2
5.8	5.8	5.8	5.8

(b) Showing all the possible 6 coincidence events in bin 5, where each 6 coincidence event can then be broken down into 5, and 4 coincidence events.

Table 2: Showing how events are binned and how every combination investigated

4.2 Results

At this point the data has been reduced from 4TB of raw data to 40GB of reduced trigger data to a few MB's of event data. This gives over 10^10 events. With most of these being not real events, as often there is a high probability that on at least one channel there will be a random noise channel. These should however be reduced by making cuts on what events reconstruct and if they reconstruct to a vertex in the water volume. It was decided to only look at trigger type

4 for this early analysis. For trigger type 4, there are 87,249,776 events that pass the causality check. 15,024,299 give real vertices, and cutting on a χ^2 of a 100, and of these events keeping only the ones that are in the water volume.

- 123,330 five-fold events
- 74,839 six-fold events
- 24,830 seven-fold events
- 9,555 eight-fold events
- Giving a total of 232,554

Figure 8 shows the x, y, and z distributions of the data.

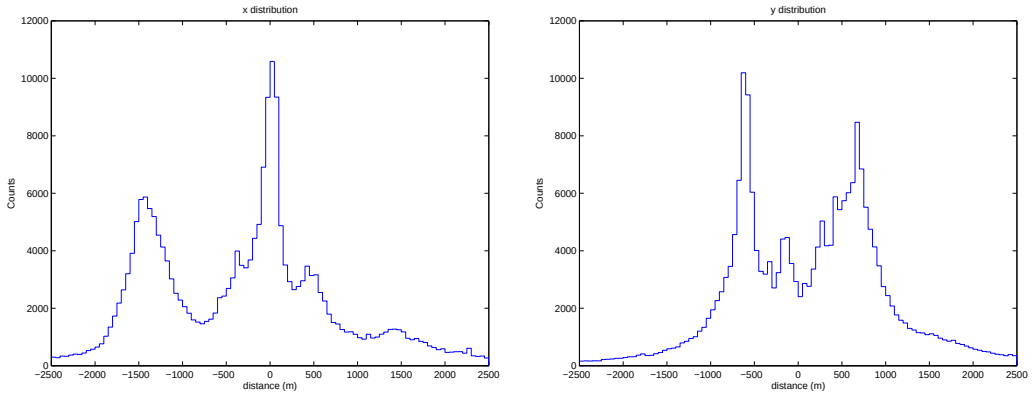

(a) x co-ordinate distribution

(b) y co-ordinate distribution

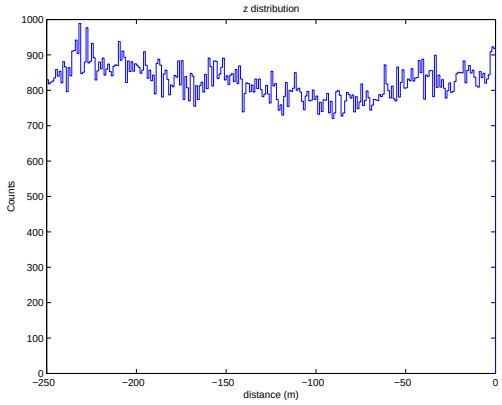

(c) z co-ordinate distribution

Figure 8: x, y, and z distributions of the events

Figure 8 shows that the z distribution is flat, so it is interesting to look at the distribution in the xy plane. Figure 9 shows this.

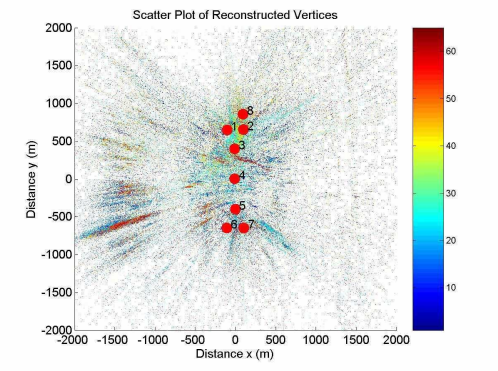

Figure 9: xy scatter plot for 5 fold coincidences for trigger type 4, where the colour represents the hit hydrophone

4.3 Preliminary Analysis

It would be expected that the z distribution have structure. It would be expected that there should be a definite peak at the sea surface. But the graph shows otherwise. The distribution looks flat, fig 8. However figure 8 shows that the x and y distributions have definite structure. What has caused this structure? Are the peaks showing the geography of the area (i.e are we seeing reflections from physical structures), are they showing places of high biological noise, or are they simply showing mathematical instability in the reconstruction algorithm? The array is not ideally shaped, 6 out of the 8 hydrophones lie on the same plane, which if only the planar hydrophones are hit, could cause massive instabilities in the reconstruction algorithm. But it can be said that it is definitely not random, the statistics are too high.

Compare this to fig 9, a 2d projection of the data. Fig 9 shows definite banding, and a left right asymmetry. At around -1500m in x there appears to be a dense region spanning y between -1000m and 1000m. Comparing the co-ordinates of this region with a topological map of the area, the dense region of events appear to corresponds to a sea cliff. Unfortunately, looking at the waveforms of the events, there still seems to be many events with a signal on most channels, but noise on others, fig 10, and hence any analysis must be treated very sceptically. More reduction must be performed on the data. It is estimated that only 10% of these 200,000 events are real.

4.4 Event Viewer and Golden Event Analysis

How do we reduce these events even further so as to only get real events? It was decided to search for golden events, events which fire on a large number of hydrophones and have a definite shape above the noise, and look at the χ^2 and the x,y,z of these events. To aid in the search for these golden events, an event displayer was created. This allowed event x, where x is the event number, to be looked at, or events to be searched through incrementally or decrementally from a given starting point. It also allows the user to store the event if they think that it is a golden event. To aid in the search for the golden event, for each event that was displayed the χ^2 value and the spherical polar co-ordinate r were displayed on the screen. Events starting from the last 8 fold coincidence and working backwards were examined. 1500 golden events were identified. Fig 10 show examples of the viewer and a golden event.

Looking at these golden events it was decided that a sensible cut would be :

$\chi^2 < 5$n, where n is the n-fold coincident event. And also an $r^2 <$ 1e6.

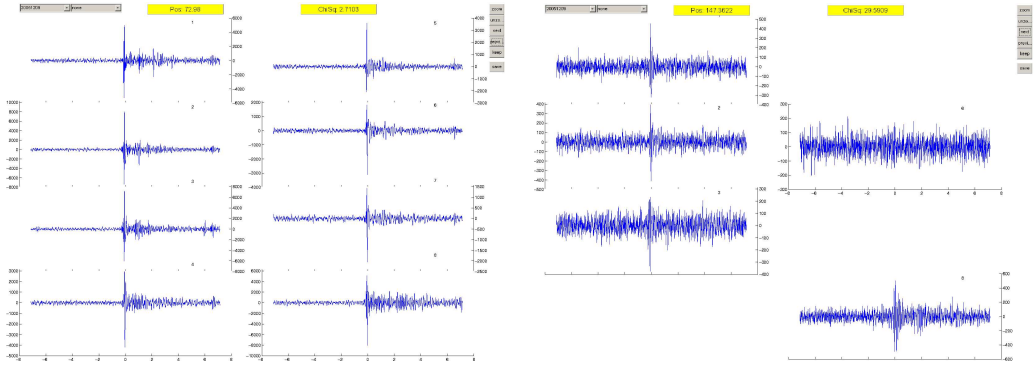

(a) A Golden Event as seen in the event viewer

(b) A Golden Event as seen in the event viewer, but this time also showing a 4 coincident event with one channel of noise

Figure 10: Golden Events as seen in the event viewer

The χ^2 is increased with n, as the more hydrophones that are hit, the greater the sum of the time differences, see appendix B. The r was decided at <1000m as the smaller the r, the less difference in reconstruction a higher χ^2 makes. This proved unsuccessful in that there are still events with noise present.

5 Why do we Need to Know the Array Position?

Consider a hydrophone that has moved by just 1 meter. On a string that has a hydrophone 132m above the seabed, this is only an angular shift of $7.58.10^{-3}$ degrees. This is a realistic shift, especially in tidal areas like the area around the Rona array. Another way of looking at this shift, is that a 1m shift, with a speed of sound of $1500ms^{-1}$, gives a difference in timing between the expected time, and the actual time of $\frac{2}{3}.10^{-3}$s, well within the sampling rate, $7.14.10^{-6}$.

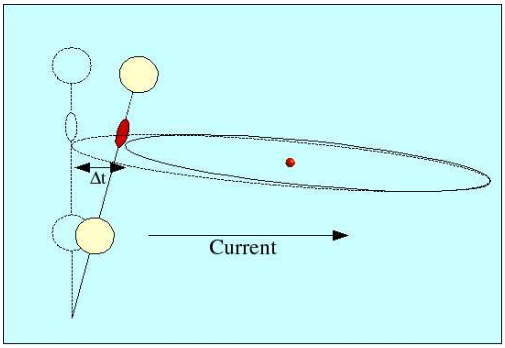

Figure 11: The effect of a correct in the hydrophones

6 The Effect of Scattering an Array

6.1 Using Monte Carlo Generated Data

To scatter the array, a Gaussian with a sigma of 1 (68% of scatters will be 1 metre or less) was applied separately to each of the x, y, and z co-ordinates of each hydrophone. This is not realistic, where you would expect some correlation to the displacement, but serves the purpose of generating unknown hydrophone co-ordinates.

From these hit times, the events were reconstructed. But instead of using the unscattered array, the scattered array was used. Figs 12 show the results of doing this.

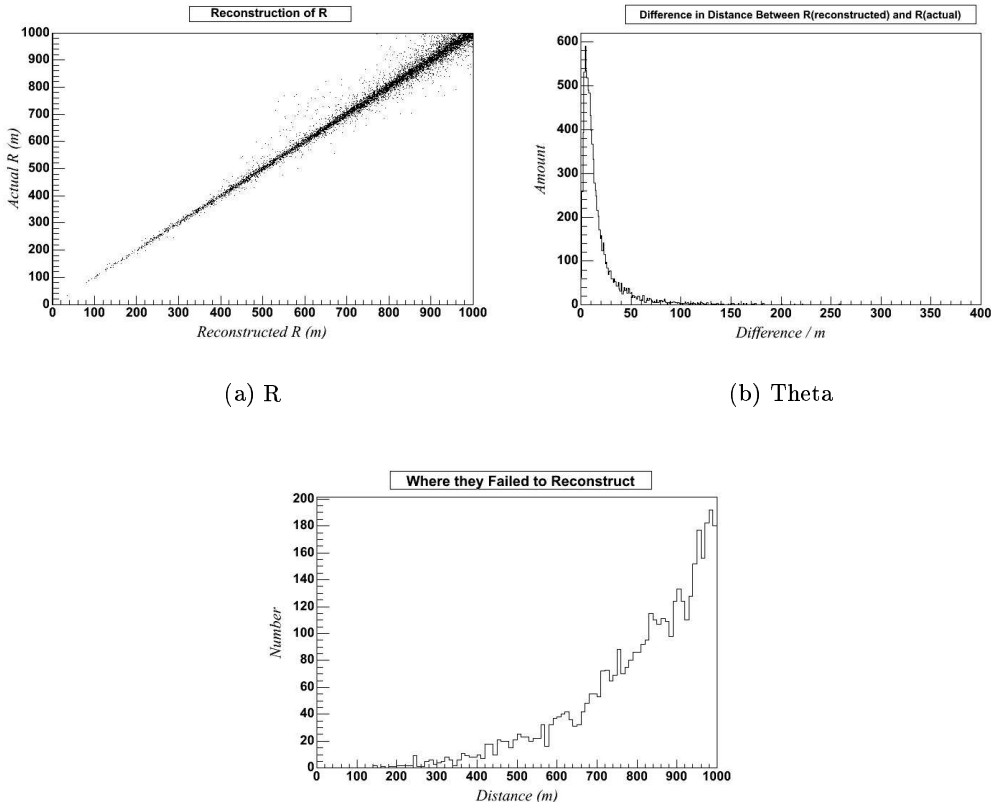

(a) R

(b) Theta

(c) Phi

Figure 12: The effect of scattering hydrophones on reconstructing a vertex

I ask how many of the events reconstruct to a given tolerance. I compare the reconstructed R to the actual R, and ask how many reconstruct to within 10m of the actual event - 48%.

6.2 Using Data from the Rona Array

The first reconstructed event from the Rona data was selected. **(438.957, 516.284, 44.0139)**

Again it is interesting to investigate what would happen if this wasn't the actual array position.

All of the hydrophones were scattered randomly using a Gaussian with a sigma of 1, and the position of the event reconstructed. This was repeated 500 times. Fig 13 shows the results

of this. The RMS of figure 14 shows that the error on the reconstructed position is of the order ± 10 meters.

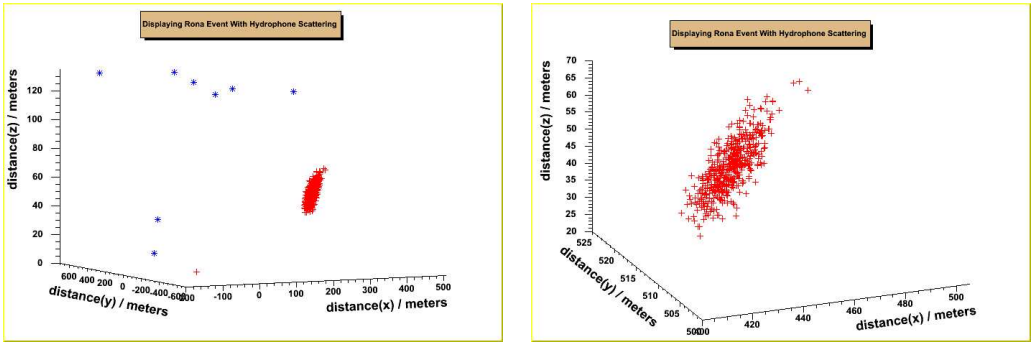

(a) the many different reconstructed positions

(b) a closer look at the positions

Figure 13: By scattering the hydrophones, many different positions are reconstructed

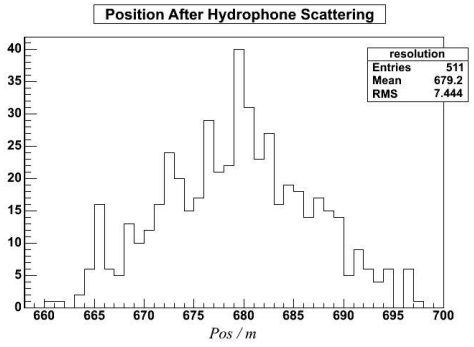

Figure 14: the distribution of the scattered array events

Therefore, can we do a multi parameter fit using noise sources to optimise the position of the array? Hence reduce the error from 10m down to cm's?.

This gives a way of calibrating the hydrophone positions without the need for external sources, and could be achieved from the data from the Rona array. It makes everything very neat. But it needs an abundant source of noise, and doesn't give an absolute energy scale calibration.

7 Finding the True Array Positions

7.1 Using Minuit

Using the Minuit package, this idea was tested to find the position of just one co-ordinate, i.e. a one parameter fit. The array was left untouched, and the noise events generated, and everything fed into the reconstruction code as normal. However this time, one of the co-ordinates was made variable, and Minuit was asked to find the value of the parameter. The minimisation was based on finding minimum χ^2, equation 18 in appendix B.

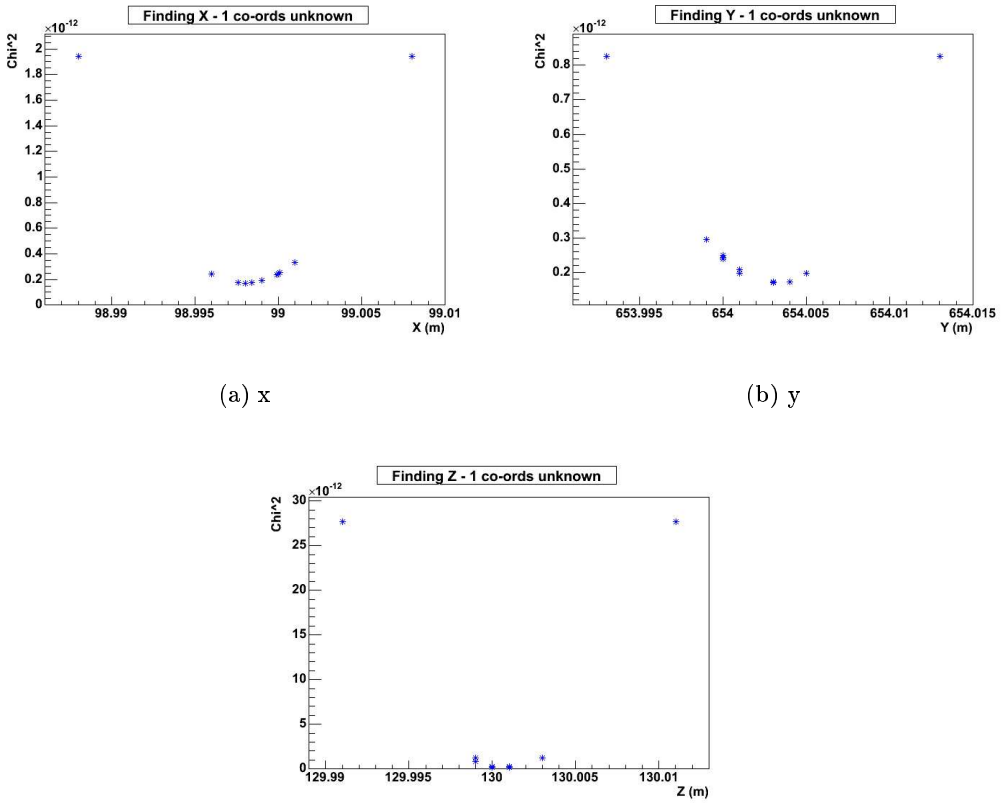

(a) x

(b) y

(c) z

Figure 15: Calculating an unknown co-ordinate for hydrophone 2, using the minimisation of the χ^2

Figs 15 show the results of this experiment. Figs 15 show a clear χ^2 curve converging on a definite value, within the accuracy that I set Minuit to find to, 0.5mm. This experiment was repeated for varying values of the unknown co-ordinate.

	x	y	z
original	-8.0	397.0	32.0
scattered	-8.9	397.0	32.0
calculated	-8.90	397.0	32.0
scattered	-6.7	397.0	32.0
calculated	-6.71	397.0	32.0
scattered	-9.3	397.0	32.0
calculated	-9.29	397.0	32.0

Table 3: scattering one co-ordinate of hydrophone 3

The next step was to try two then three (a hydrophone) unknown parameters.

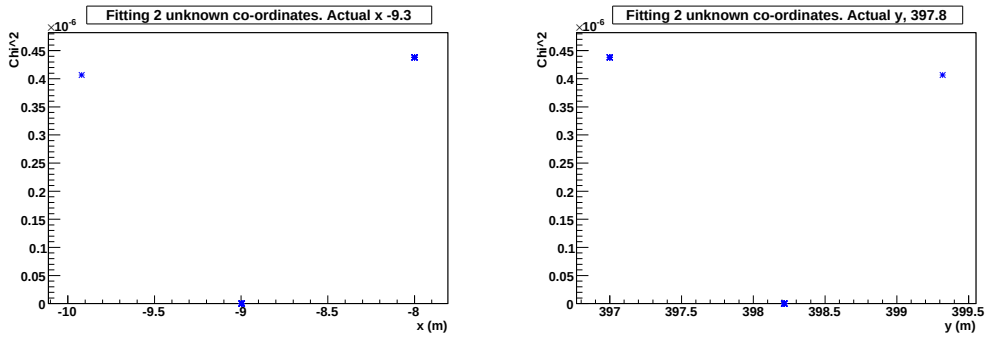

(a) the χ^2 plot for x with two unknown parameters

(b) the χ^2 plot for y with two unknown parameters

Figure 16: Calculating two unknown parameters using the minimisation of the χ^2

Figs 16 show an example of a typical output from a 2 parameter optimisation. A smooth curve was never seen, and the minimisation often finished after very few attempts. Although fig 16 has more than the obvious 3 points. These are always clustered around the 3 points that can be seen. After finishing the minimisation, the minimum that Minuit returns, consistently came back with results that were greater than 0.5 meters away from the actual position. This wasn't promising, something is clearly wrong.

7.2 Looking at the error surface

Why didn't this minimisation work? There is a definite solution to the minimisation, and there are only a small number of parameters to optimise. The first step was to investigate the error surface. This was examined in 2 parameter space. The χ^2 was calculated over a parameter space ± 5 meters from the actual answer every 10cm, and the results stored in a histogram.

Figure 17 shows the plot of χ^2 over 2 dimensional parameter space for one noise source. This clearly shows the problem that Minuit was having. It doesn't appear to have one clear minimum. It isn't a well, it's more of a valley. Minuit was not finding the wrong answer, it

was just that the system was severely under-constrained, and Minuit was simply telling me this. How do you over come this problem? It was solved by repeating the exercise but for many noise sources, and building up error surface so that it has a clear minimum, fig 17.

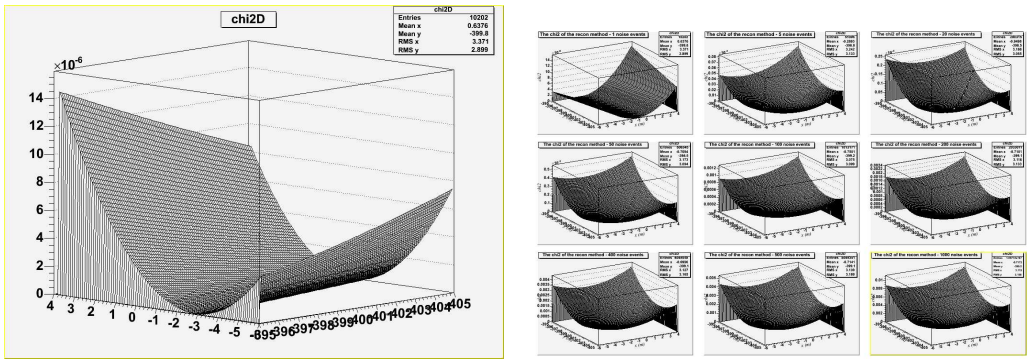

(a) Looking at the error surface in 2 parameter space

(b) Building up the error surface

Figure 17: The Error Surface

The minimum was then found by finding the bin with the smallest value. This worked for up to a three parameter fit, a hydrophone, to the tolerance of the parameter space, in this case, 5cm. As an example, building up an error surface with 100 noise events. Hydrophone 7 was scattered, whilst keeping the other hydrophones constant, table 4

	x	y	z
original	105.0	-648.0	132.0
scattered	105.6	-648.3	131.0
calculated	105.64	-648.25	131.06

Table 4: finding an unknown hydrophone

This shows that it is possible to fit for at least one hydrophone, but calculating the minimum of an error surface is a highly inefficient way of doing this. Fitting programmes need to be reintroduced.

7.3 Optimising for Many Noise Sources

However Minuit failed when many hydrophones had to be optimised. A new technique was then decided upon. Firstly, the z co-ordinate was fixed. This was decided as, the z drift is insignificant over the distances considered here, and hydrophone 8 was fixed. This is because hydrophone 8 is fixed to the seabed. Again Minuit failed. The same technique was now tried using Matlab. This time the results were as would be hoped for. Scattering the hydrophones in x, y, and z randomly by 100m, the optimisation found each hydrophone location to within $1\text{x}10^{-3}$m in 50.0 seconds.

This technique was then applied to the Golden Events. The idea that, for each 10 minute file, the events could be found, the array optimised using the found events, and then the vertexes reconstructed using the optimised array. Fig 18 shows the result of this for the two weeks of data for the x co-ordinate.

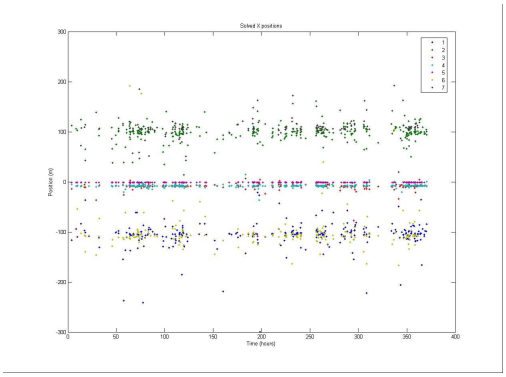

Figure 18: The optimisation results for the x co-ordinate

Sadly fig 18 shows no correlation. It would be hoped for that the hydrophones would show a diurnal fluctuation in tide movement, or show no movement at all (as the hydrophones are quite deep, and the tidal movement is mainly a surface effect). It would be hoped that from the result of this, a function could be developed, so that the array could be automatically optimised according to the tidal state. But as has been stated before, the data is still not fully reduced into a sensible state, and many of the golden events still contain noise, and are possibly not actually genuine events.

8 Future Work

The immediate future is to reduce the data into a set of pure actual events, with no noise events represented. The idea is to use a pattern matching technique. Each event will be looked at, and the wave form analysed. This will remove channels which contain noise, and only keep the signal channels. Re-applying the cuts, only actual events will be kept. From this, the optimisation code can then be re-applied, the array optimisation performed, and then the vertex reconstruction performed. This will then provide a map of real events.

Another analysis that will be performed very shortly is a FFT of the data. For random noise/events, the power spectrum will be flat. But for a noise on a longer time scale peaks will be expected. Noise that will be expected of this type will be ships. Therefore using the results from the FFT, can we plot the trajectory of ships?

Longer terms plans are to continue the analysis of the Rona data. ACoRNE has recently purchased a tape deck, and within the next two months there will be a continuous stream of data to analyse. Using this data better signal processing needs to be developed, more efficient algorithms, better random noise discrimination and coincidence logic, array optimisation, and improved event displaying. What also ties in with this work is the need for more accurate reconstruction algorithms. Diffraction, reflection or complex attenuation has yet to be considered. Also pointing and energy estimation algorithms need to be developed.

This will lead to a better understanding of the background noise. Can we start to see clustering of events, can we map the topology of the area, especially the surface, can we track the movement of biology, can we begin to recognise waveforms? Only then can we discriminate against it, leaving a clean background for a UHE neutrino pulse.

There is also work to be done on calibrating the array using an artificial dipolar noise source. Understanding the noise background and having an accurate reconstruction algorithm will be vital for this work. Then once the array and the background is understood, the ultimate conclusion from this is to publish a upper limit of the flux for UHE neutrino detection using acoustic techniques.

Using this information on how a real array performs, work will be begin in investigating designs for future acoustic arrays.

The work described above will form a large chunk of my PhD thesis.

References

[1] Christian Spiering. High energy neutrino astronomy. the experimental road. *astro-ph*, 4, 2003, arXiv:astro-ph/0303068.

[2] N.G Lehtinen. Sensitivity of an underwater array to ultra high energy neutrinos. *Astropart. Phys. 17*, 279, 2002, arXiv:astro-ph/0104033.

[3] Pietro Ubertini. The integral - hess/magic. *astro-ph*, 2006, arXiv:astro-ph/0605228.

[4] Todor Stanev. High energy neutrinos: Sources and fluxes. *astro-ph*, 2005, arXiv:astro-ph/0511641.

[5] E. Waxman and J. Bachcall. High energy astrophysics. *Phys. Rev.*, D59, 1999.

[6] Mannheim, Protheroe, and Rachen. Waxman-bachall limit. *Ap. J*, 199, 2000, arXiv:astro-ph/9812398.

[7] G. Patanchon, J. Delabrouille, and J.-F. Cardoso. Astrophysical data sets from the wmap satellite. *astro-ph*, 4, 2004, arXiv:astro-ph/0403363.

[8] J. G. Learned and Karl Mannheim. High energy neutrino astrophysics. *Annual Review Nuclear and particle Science*, 50, 2000.

[9] Henri, Pelletier, Petrucci, and Renaud. Active galactic nuclei as high energy engines. *astro-ph*, 1999, arXiv:astro-ph/9901051.

[10] Engel, Seckel, and Stanev. Neutrinos from propagation of ultra-high energy protons. *astro-ph*, 2001, arXiv:astro-ph/01012116.

[11] Amanda. Limits on diffuse fluxes of high energy extraterrestrial neutrinos with the amanda-b10 detector. *astro-ph*, 2003, arXiv:astro-ph/0303218.

[12] Amanda. Search for extraterrestrial point sources of neutrinos with amanda-ii. *Physical Review letters*, 92, 2004.

[13] Paolo Lipari. Prospectives of high energy neutrino astonomy. *astro-ph*, 2006, arXiv:astro-ph/0605535.

A Deriving the Reconstruction Matrix

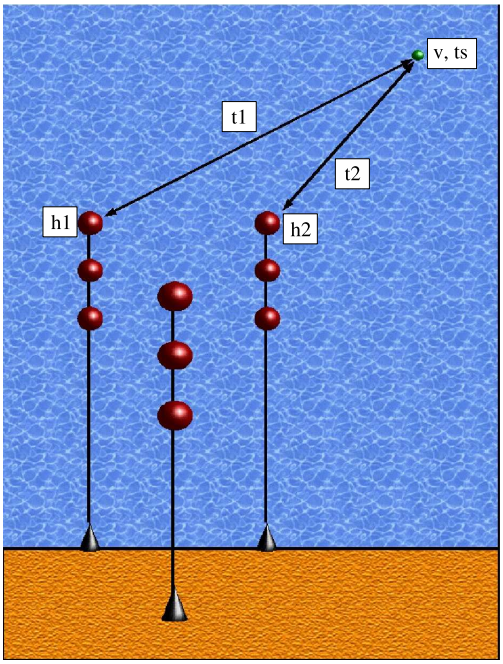

Figure 19: A schematic showing the parameters needed for reconstruction

$\vec{\nu} = (\nu_x, \nu_y, \nu_z)$ the shower location : UNKNOWN
$\vec{r_i} = (x_i, y_i, z_i)$ location of hydrophone i : KNOWN
t_i time measured at hydrophone i : KNOWN
t_s time of shower : UNKNOWN
c = 1500ms $^{-1}$ the speed of sound in water : KNOWN

First consider the equation of distance = speed x time. For the geometry that I am considering this becomes :

$$|\vec{\nu} - \vec{r_i}| = c^2 (t_i - t_s) \tag{3}$$

Now square this, and take the difference between the time it takes the shower to arrive at two different hydrophones.

$$|\vec{\nu} - \vec{r_i}|^2 = c^2 (t_i - t_s)^2 \tag{4a}$$
$$\nu^2 + r_i^2 - 2\vec{\nu} \cdot \vec{r_i^2} = c^2 (t_i - t_s)^2 \tag{4b}$$
$$\left(r_i^2 - r_j^2\right) - c^2 \left[(t_i - t_s)^2 - (t_j - t_s)^2\right] = 2\vec{v} \cdot (\vec{r_i} - \vec{r_j}) \tag{4c}$$
$$\left(r_i^2 - r_j^2\right) - c^2 \left[t_i^2 - t_j^2 - 2t_s (t_i - t_j)\right] = 2\vec{v} \cdot (\vec{r_i} - \vec{r_j}) \tag{4d}$$
$$\left(r_i^2 - r_j^2\right) - c^2 \left[t_i^2 - t_s j 2\right] - 2c^2 (t_i - t_j) = 2\vec{v} \cdot (\vec{r_i} - \vec{r_j}) \tag{4e}$$

If this is done for many hydrophones, the problem becomes a matrix problem. With the matrix equation looking like :

$$\vec{R} + t_s \vec{T} = M \times \vec{\nu} \tag{5}$$

Where :

$$\vec{R} = \{r_i^2 - r_j^2 - c^2\left(t_i^2 - t_j^2\right)\}; (i, j = 1, 2; 1, 3; 1, 4) \tag{6}$$

$$\vec{T} = \{2c^2\left(t_i - t_j\right)\}; (i, j = 1, 2; 1, 3; 1, 4) \tag{7}$$

$$M = 2\begin{pmatrix} dx_{12} & dy_{12} & dz_{12} \\ dx_{13} & dy_{13} & dz_{13} \\ dx_{14} & dy_{14} & dz_{14} \end{pmatrix} \tag{8}$$

This can be extended for every hydrophone that has been hit. Where hydrophone 1 in the equations above can be any hydrophone. The shower location is hence :

$$\vec{\nu} = M^{-1} \times \left(\vec{R} + t_s\vec{T}\right) \tag{9}$$

$$\vec{\nu} = M^{-1}\vec{R} + t_s M^{-1}\vec{T} \tag{10}$$

Group the known and unknown parts of the equation 9

$$\vec{P} = M^{-1}\vec{R} \tag{11}$$

$$\vec{Q} = M^{-1}\vec{T} \tag{12}$$

So now the shower location becomes :

$$\vec{\nu} = \vec{P} + t_s\vec{Q} \tag{13}$$

Where all is known except t_s. To solve for this, again consider equation 3. Using equation 13, $\vec{\nu}$ can be replaced. This gives a quadratic in t_s, which can be solved for any hydrophone that has hit :

$$|\vec{\nu} - \vec{r}_i|^2 = c^2\left(t_i - t_s\right)^2 = \left|\vec{P} + t_s\vec{Q} - \vec{r}_i\right|^2 \tag{14}$$

$$t_s^2\left(c^2 - Q^2\right) - 2t_s\left(c^2 t_i + \vec{P}\cdot\vec{Q} + \vec{Q}\cdot\vec{r}_i\right) + \left(c^2 t_i^2 - p^2 - r_i^2 + 2\vec{P}\cdot\vec{r}_i\right) \tag{15}$$

A.1 Minimum number of Hydrophones

The minimum number of hydrophones that have to be hit for this technique to work is four. If any less than this are hit the solution becomes ambiguous. Figure 20 shows why this would be the case.

It is clear to see that by having only three hydrophones, there are two equally valid solutions. By having four, this ambiguity is removed, and one solution can be achieved. Although if the four hydrophones are in a plane, the same problem still exists.

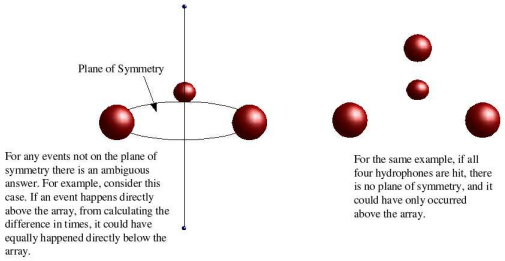

Figure 20: Showing the minimum number of hydrophones

A.2 Inverting the M

If M is singular (the determinant is zero), or if the system is over constrained (more than four hits), M cannot be inverted using using normal matrix inversion techniques. Instead a technique called singular value decomposition has to be used (SVD).

For every m $\times$ n matrix, if m $\geq$ n, the matrix can be written as

$$M = ULV^T \tag{16}$$

Where U and V are orthogonal matrices, containing the column and row eigenvector respectively, and L is a diagonal matrix containing the eigenvalues in decreasing order. Inverting this is simple :

$$M^{-1} = VL^{-1}U^T \tag{17}$$

Where L^{-1} is simply a matrix of the inverse of each element.

Using this technique, every matrix can be inverted.

B The Solutions of the Quadratic

As with all quadratics there are two solutions, a positive and a negative root. One right answer, one wrong. But the question was asked, which solution is correct?

- Positive Root - No, only ~50% of events reconstruct
- Negative Root - No, only ~50% of events reconstruct
- Earliest root - Better, but still only ~75% of events reconstruct
- Taking the Chi Squared - >99% reconstruct

The χ^2 test - The chi squared test is a test comparing the difference of the actual hit times, and the reconstructed hit times, and taking the euclidean norm of the result. By looking for the smallest χ^2 value the correct root can be chosen.

$$\chi^2 = \left(t_i\left(actual\right) - t_i\left(recon\right)\right)^2 \tag{18}$$

The reconstructed time for either the positive or negative root is defined as.

$$t_i\left(recon\right) = \left(t_{s(\pm)} + \left(h_i - v_{s(\pm)}\right)/c\right) \tag{19}$$

In equation 19, an imaginary signal is propagated backwards from each of the calculated positions, the plus or minus solutions from equation 14, and substituting the time into equation 13. Starting at the calculated time , again the corresponding plus or minus solution from equation 14, and using the speed of sound in water, the time that it hits a specified hydrophone can then be calculated. This can be compared to the time the hydrophone was actually hit. The vertex that corresponds to the smallest χ^2 is then the preferred solution.

Why is one solution wrong? - The initial system of equations is built up using the squared times, so it doesn't take into account cases where the transit time has got the wrong sign.

C Adapting the χ^2 test for multiple noise sources

As described in section 7.2 the error surface has to be built up using multiple noise events. Therefore when optimising the array, the minimisation looks for a minimum χ^2 of multiple noise events. This involves a slight modification to equation 18.

Now instead of just finding the difference between the actual and reconstructed time for just one hydrophone. We will instead calculate the difference between the reconstructed value and the actual values a little more accurately.

$$\chi^2 = sum(|diff(c \times t) - diff(\vec{h} - \vec{v})|) \tag{20}$$

c = speed of sound in water
t = hit hydrophone times
$\vec{h}$ = hydrophone locations (of hit hydrophones)
$\vec{v}$ = reconstructed vertex position

Where the difference is described as:

$$diff = r_{h2} - r_{h1}, r_{h3} - r_{h2}, \ldots r_{h8} - r_{h7} \tag{21}$$

nb only for the hit hydrophones, not always all of the hydrophones

Equation 20 redefines the χ^2 function ready for multiple noise calculations. Instead of just comparing the difference in reconstructed and actual times on a single given hydrophone, we now compare the difference in lengths between adjacent hydrophones in the array, for the reconstructed vertex and the actual hit times.

Now for multiple noise events, the χ^2 simply becomes the sum of all the individual χ^2 for each noise event. For the optimisation of the array, it is this sum of χ^2 that is minimised.